HAL open science

Assessment of shape-based features ability to predict the ascending aortic aneurysm growth

Leonardo Geronzi, Pascal Haigron, Antonio Martinez, Kexin Yan, Michel Rochette, Aline Bel-Brunon, Jean Porterie, Siyu Lin, Diana Marcela Marin-Castrillon, Alain Lalande, et al.

To cite this version:

Leonardo Geronzi, Pascal Haigron, Antonio Martinez, Kexin Yan, Michel Rochette, et al.. Assessment of shape-based features ability to predict the ascending aortic aneurysm growth. Frontiers in Physiology, 2023, 14, pp.1125931. 10.3389/fphys.2023.1125931 . hal-04060967

HAL Id: hal-04060967

https://hal.science/hal-04060967

Submitted on 30 May 2023

HAL is a multi-disciplinary open access archive for the deposit and dissemination of scientific research documents, whether they are published or not. The documents may come from teaching and research institutions in France or abroad, or from public or private research centers.

L'archive ouverte pluridisciplinaire **HAL**, est destinée au dépôt et à la diffusion de documents scientifiques de niveau recherche, publiés ou non, émanant des établissements d'enseignement et de recherche français ou étrangers, des laboratoires publics ou privés.

Distributed under a Creative Commons Attribution 4.0 International License

frontiers | Frontiers in Physiology

TYPE Original Research
PUBLISHED 06 March 2023
DOI 10.3389/fphys.2023.1125931

Check for updates

OPEN ACCESS

EDITED BY
Estefania Peña,
University of Zaragoza, Spain

REVIEWED BY
Seungik Baek,
Michigan State University, United States
Alessio Gizzi,
Campus Bio-Medico University, Italy

*CORRESPONDENCE
Leonardo Geronzi,
leonardo.geronzi@uniroma2.it

SPECIALTY SECTION
This article was submitted to Computational Physiology and Medicine, a section of the journal Frontiers in Physiology

RECEIVED 16 December 2022
ACCEPTED 24 February 2023
PUBLISHED 06 March 2023

CITATION
Geronzi L, Haigron P, Martinez A, Yan K, Rochette M, Bel-Brunon A, Porterie J, Lin S, Marin-Castrillon DM, Lalande A, Bouchot O, Daniel M, Escrig P, Tomasi J, Valentini PP and Biancolini ME (2023), Assessment of shape-based features ability to predict the ascending aortic aneurysm growth.
Front. Physiol. 14:1125931.
doi: 10.3389/fphys.2023.1125931

COPYRIGHT
© 2023 Geronzi, Haigron, Martinez, Yan, Rochette, Bel-Brunon, Porterie, Lin, Marin-Castrillon, Lalande, Bouchot, Daniel, Escrig, Tomasi, Valentini and Biancolini. This is an open-access article distributed under the terms of the Creative Commons Attribution License (CC BY). The use, distribution or reproduction in other forums is permitted, provided the original author(s) and the copyright owner(s) are credited and that the original publication in this journal is cited, in accordance with accepted academic practice. No use, distribution or reproduction is permitted which does not comply with these terms.

Assessment of shape-based features ability to predict the ascending aortic aneurysm growth

Leonardo Geronzi[1,2]*, Pascal Haigron[3], Antonio Martinez[1,2], Kexin Yan[2,4], Michel Rochette[2], Aline Bel-Brunon[4], Jean Porterie[5], Siyu Lin[6,7], Diana Marcela Marin-Castrillon[6,7], Alain Lalande[6,7], Olivier Bouchot[8], Morgan Daniel[3], Pierre Escrig[3], Jacques Tomasi[3], Pier Paolo Valentini[1] and Marco Evangelos Biancolini[1]

[1]Department of Enterprise Engineering "Mario Lucertini", University of Rome Tor Vergata, Rome, Italy, [2]Ansys France, Villeurbanne, France, [3]LTSI–UMR 1099, CHU Rennes, Inserm, University of Rennes, Rennes, France, [4]LaMCoS, Laboratoire de Mécanique des Contacts et des Structures, CNRS UMR5259, INSA Lyon, University of Lyon, Villeurbanne, France, [5]Cardiac Surgery Department, Rangueil University Hospital, Toulouse, France, [6]IMVIA Laboratory, University of Burgundy, Dijon, France, [7]Medical Imaging Department, University Hospital of Dijon, Dijon, France, [8]Department of Cardio-Vascular and Thoracic Surgery, University Hospital of Dijon, Dijon, France

The current guidelines for the ascending aortic aneurysm (AsAA) treatment recommend surgery mainly according to the maximum diameter assessment. This criterion has already proven to be often inefficient in identifying patients at high risk of aneurysm growth and rupture. In this study, we propose a method to compute a set of local shape features that, in addition to the maximum diameter *D*, are intended to improve the classification performances for the ascending aortic aneurysm growth risk assessment. Apart from *D*, these are the ratio *DCR* between *D* and the length of the ascending aorta centerline, the ratio *EILR* between the length of the external and the internal lines and the tortuosity *T*. 50 patients with two 3D acquisitions at least 6 months apart were segmented and the growth rate (GR) with the shape features related to the first exam computed. The correlation between them has been investigated. After, the dataset was divided into two classes according to the growth rate value. We used six different classifiers with input data exclusively from the first exam to predict the class to which each patient belonged. A first classification was performed using only *D* and a second with all the shape features together. The performances have been evaluated by computing accuracy, sensitivity, specificity, area under the receiver operating characteristic curve (AUROC) and positive (negative) likelihood ratio LHR+ (LHR–). A positive correlation was observed between growth rate and *DCR* (r = 0.511, p = 1.3e-4) and between GR and *EILR* (r = 0.472, p = 2.7e-4). Overall, the classifiers based on the four metrics outperformed the same ones based only on *D*. Among the diameter-based classifiers, k-nearest neighbours (KNN) reported the best accuracy (86%), sensitivity (55.6%), AUROC (0.74), LHR+ (7.62) and LHR– (0.48). Concerning the classifiers based on the four shape features, we obtained the best accuracy (94%), sensitivity (66.7%), specificity (100%), AUROC (0.94), LHR+ ($+\infty$) and LHR– (0.33) with support vector machine (SVM). This demonstrates how automatic shape features detection combined with risk

classification criteria could be crucial in planning the follow-up of patients with ascending aortic aneurysm and in predicting the possible dangerous progression of the disease.

KEYWORDS

cardiovascular diseases, ascending aorta aneurysm, biomechanical features, classification, aorta, machine learning, growth rate, risk assessment

1 Introduction

Ascending aortic aneurysm (AsAA) is a risky dilatation of a weakened area of the ascending aorta (AAo) which may lead to dissection or rupture (Guo et al., 2018). Unfortunately, it is generally a silent pathology and the first symptoms may already indicate a serious and late-stage clinical situation with severe, life-threatening internal bleeding (Papagiannis, 2017). The estimated pooled incidence is between 5 and 10/100,000 individuals per year (Kuzmik et al., 2012; Melo et al., 2021). To date, the main criterion for elective ascending aortic surgery of non-urgent cases is the maximum diameter assessment whose decision threshold is generally fixed at 55 mm (Anfinogenova et al., 2022). Unfortunately, this does not seem to correctly reflect the AsAA patient's risk of rupture (Elefteriades and Farkas, 2010; Tozzi et al., 2021) and is often considered insufficient as criterion of choice (Sonsino et al., 2022). In fact, many studies show aneurysms with diameters below the threshold for elective surgery which experience rupture while other aortas with huge diameters remain stable over time in terms of size (Smoljkić et al., 2017). Recently, the aneurysm growth rate (GR) (Oladokun et al., 2016) has also been included as a decision criterion for elective surgery. Therefore, as further stated in the clinical guidelines (Members et al., 2014), patients with rapid growth of the aortic diameter (more than 3 mm/year) should be considered for preventive surgical replacement. Furthermore, the process of aneurysm growth seems to be accelerated by the presence of a bicuspid aortic valve and congenital pathologies (Davies et al., 2007). For these reasons, the research is now focused on determining new biomarkers (Califf, 2018) for early diagnosis that can predict the aneurysm evolution and allow an accurate risk assessment. Some of those proposed have been associated to the shape of the aneurysm (Lindquist Liljeqvist et al., 2021) and mainly introduced for the abdominal aorta aneurysm (AAA). Among the measures related to the AAA shape, the vessel tortuosity and asymmetry seem to be highly relevant for predicting the rupture (Pappu et al., 2008; Doyle et al., 2009). According to Grobman and Stamilio (2006), the identification of local features on the shape of the abdominal aorta is valuable in assessing the risks of aneurysm rupture and establishing index thresholds for selecting patients to be surgically treated. An interesting framework describing the steps for a robust characterization of vascular geometries was proposed by Piccinelli et al. (2009) and applied to cerebral aneurysms. Here, all the steps from the image segmentation to the geometric characterization of the vascular structure are shown. The possibility of using algorithms to identify higher-risk patients has already been widely discussed (Saeyeldin et al., 2019). Shum et al., using a retrospective dataset of 76 patients, estimated geometric indices and regional variations in wall thickness and presented a decision tree algorithm to classify the data according to rupture criteria (Shum et al., 2011). Lee et al. (2013) proposed a classifier based on statistical machine learning for the curvature features of the abdominal aorta to evaluate the risk of rupture while Rengarajan et al. (2020) integrated biological information with geometric data to assess the same risk. Concerning the AsAA, the importance of estimating the length of the ascending tract for the decision of surgery has been demonstrated (Krüger et al., 2016; Wu et al., 2019). Kruger et al. presented a risk score based on the centerline length and on the maximum diameter (Krüger et al., 2018). Additionally, Poullis et al. (2008) showed how higher curvatures of the ascending aorta corresponded to higher forces exerted on the wall, explaining the potential effect this feature may have on the risk of aortic dissection. The AsAA risk of rupture has been assessed by considering also indices deriving from the ratio of the patient's diameter and the height or body surface area (Zafar et al., 2018). Liang et al. (2017) presented a machine learning approach to evaluate a risk score for some patients previously tested with a structural simulation that brought the model to rupture. Jiang et al. (2020), using abdominal aortic aneurysm longitudinal data, Growth and Remodeling (G&R) techniques and Probabilistic Collocation Method (PCM), demonstrated how the diameter evolution over time can be better predicted using Deep Belief Network (DBN) compared to classical non-linear mixed-effect models (Sweeting and Thompson, 2012). Kim et al. (2022) used convolutional neural networks (CNNs) to predict the abdominal aortic aneurysm growth by integrating information of the vessel radius, thrombus thickness, Time Averaged Wall Shear Stress (TAWSS) derived from fluid-dynamic simulation and information of the exponential growth rate.

In this paper, we propose a method to obtain shape features to identify patients at high risk of AsAA growth. Besides the diameter, already proposed in the guidelines, these are the ratio between the diameter and the centerline length, the ratio between the length of the external and internal lines and the tortuosity of the ascending tract. Using longitudinal data derived from 50 patients, we segmented each image dataset to obtain a patient-specific geometry. After, we investigated the correlation between each shape feature computed on the first exam and the aneurysm growth rate calculated by exploiting the two acquisitions. Finally, using the shape features computed for the first exam only, we used and compared six different machine learning (ML) classifiers in order to predict the patients that could present adverse and fast AsAA evolution and show how these new local features can complement the information currently provided by the diameter alone.

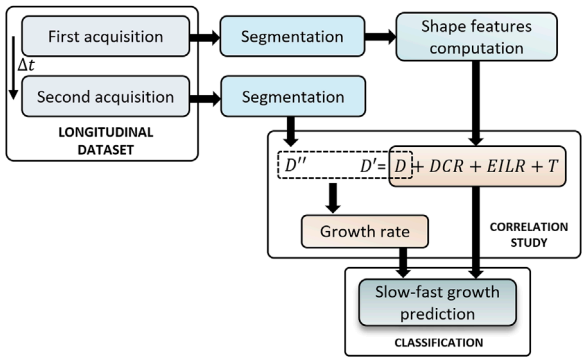

FIGURE 1
Full workflow for identifying patients at high risk of aneurysm growth.

2 Materials and methods

The full pipeline of this study is presented in **Figure 1**. The current section is structured as follows: in **Section 2.1** the dataset used for this study is described. In **Section 2.2** we explain how the segmentation was performed while in **Section 2.3** the methods for obtaining the shape features are presented. After, the method to compute the growth rate is reported in **Section 2.4** and we conclude with **Section 2.5** explaining the classification methods used to predict the risk class to which each patient belongs.

2.1 Data

To compute and evaluate the shape features, we used a retrospective dataset collected from the registry systems of three centers: the University Hospital of Rennes (Rennes, France), the University Hospital of Dijon (Dijon, France) and the University Hospital of Toulouse (Toulouse, France). The study has been conducted in accordance with ethical standards. The acquisitions were performed between December 2006 and September 2022 and the dataset was previously anonymized. Only the patients with at least two pre-operative 3D exams for which the official clinical report stated a condition of dilated aorta were included. We used both CT and MRI-Angiography images removing all the image dataset for which the resolution was worse than 1 mm × 1 mm × 1 mm. Additional exclusion criteria comprised 1) patients younger than 25 years, 2) prior valvular surgery, 3) aneurysms related to an infection or systemic inflammatory disease, 4) presence of acute aortic syndrome including dissection (type A, Stanford) and intramural hematoma, 5) diagnosis of congenital tissue disorders such as Marfan syndrome (Pyeritz and McKusick, 1979) and 6) existence of artefacts in the images. For each patient, we then considered the time interval between the two available acquisitions and 7) we excluded those with less than 6 months between the two longitudinal exams. Overall, 50 subjects, for a total of 100 exams, were included: 29 patients with a double ECG-gated acquisition, 21 with at least one non-gated. The longitudinal dataset included 86 (86%) CT-Scans and 14 (14%) MRI-Angiography. 72 acquisitions (72%) were performed with contrast agent injection and 28 (28%) without. The main characteristics of the patients, including the age at the date of the first acquisition, are given in **Table 1**.

TABLE 1 Characteristics of the dataset.

	Total = 50
Males (%)	33 (66%)
Age (in years)	58.1 ± 13.2
Bicuspid valve	20 (40%)

2.2 Segmentation

For each patient, the segmentation of the whole thoracic aorta, from the aortic annulus to the descending aorta at the level of the diaphragm, was obtained using 3DSlicer (Fedorov et al., 2012). CT-Scans and MRI images were initially segmented using a semi-automatic local thresholding method (Senthilkumaran and Vaithegi, 2016) based on the grey level histogram derived from the analysis of three sets of voxels. Each set consisted of a different number of voxels (depending on the resolution of the images) distributed inside a sphere of radius 5 mm with the centre located at the middle of each of the three principal portions of the aorta: the ascending aorta, the aortic arch and the descending aorta. After extracting the 3-dimensional surface with Flying Edges algorithm (Schroeder et al., 2015), post-processing erosion and expansion methods were used to separate the structure of the aorta from other tissues and organs (Radl et al., 2022). The resulting surface underwent a manual editing process for verifying that it corresponded to the inner lumen of the vessel and for the correction of possible improperly segmented portions, especially in the case of geometries derived from MRI acquisitions. A median filter was then applied with a kernel size of 3 mm. At the end of the segmentation procedure, for each patient a tessellated surface made up of 8000–15000 triangular elements has been obtained.

2.3 Shape-based features

The geometric features we propose are all influenced by conformation, direction and length of the centerline (Dey and Zhao, 2002). It was extracted using the Vascular Modeling Toolkit (VMTK) through Voronoi diagrams (WSCG, 2003) after an automatic detection of the inlet and outlets seed points (Saitta et al., 2022). The segmented domain S related to the AAo and the corresponding centerline tract C were isolated with a first cut perpendicular to C at the level of the annulus and a second one in correspondence to the ostium of the brachiocephalic trunk. The methods to derive each shape feature are detailed below.

2.3.1 Diameter

The AAo intra-luminal diameter is measured by extracting n = 100 sections Ψ_k for $k = 1,\ldots,n$ perpendicular to C and equally spaced along it. **Figure 2A** shows one of the thoracic aorta segmentations, the isolated ascending tract and a subset of 20 sections. On each section Ψ_k, the maximum diameter D_{max_k} is obtained as the longest

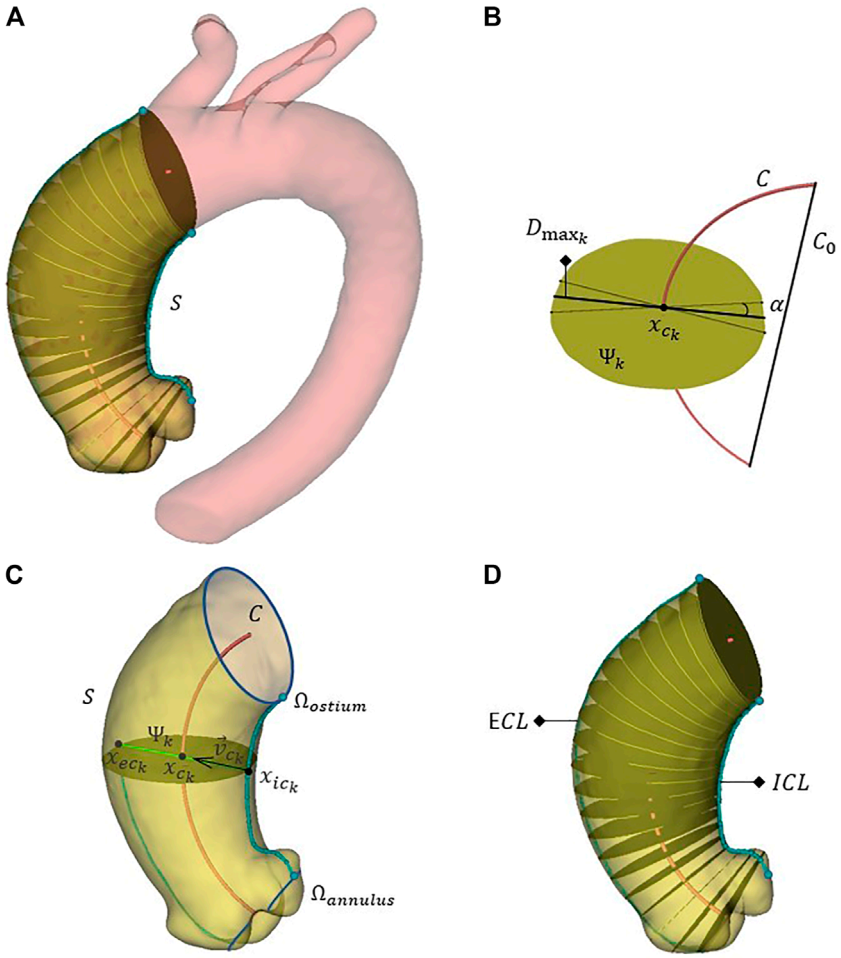

FIGURE 2
The full aorta segmentation, the discrete ascending aorta domain S and a subgroup of 20 aortic sections perpendicular to the centerline **(A)**. A generic section Ψ_k isolated for the calculation of the related maximum diameter D_{max_k}; the centerline of the ascending section C and the segment C_0 are also shown **(B)**. Identification of the point x_{ec_k} to compute the external curvature line **(C)**. Isolated ascending section with the external and internal curvature line (*ECL* and *ICL*) **(D)**.

of the segments resulting from the intersection between Ψ_k itself and a rotating a plane perpendicular to Ψ_k, passing through x_{c_k} and sweeping angles of $\alpha = 10°$ (**Figure 2B**). In turn, x_{c_k} is the point of intersection between Ψ_k and C. The maximum diameter D for the entire vessel, current main criterion for elective AAo surgery, is:

$$D = max\left\{D_{max_1}, \ldots, D_{max_n}\right\} \tag{1}$$

2.3.2 Diameter-centerline ratio

By using the maximum diameter D and computing the length of AAo centerline $\mathcal{L}(C)$, we define the diameter-centerline ratio DCR:

$$DCR = \frac{D}{\mathcal{L}(C)} \tag{2}$$

2.3.3 External-internal line ratio

Given the tessellated surface S consisting of a set F of triangular faces F_i such that any point $P \in S$ lies in at least one triangle $F_i \in F$, we can identify a polygonal curve $\Gamma_j^{x_a,x_o}$ on S starting from an arbitrary point $x_a \in \Omega_{annulus}$ and reaching another arbitrary point $x_o \in \Omega_{ostium}$ where $\Omega_{annulus}$ and Ω_{ostium} are respectively the boundaries of S at the level of the annulus and at the level of the ostium. The length $\mathcal{L}(\Gamma_j^{x_a,x_o})$ is:

$$\mathcal{L}\left(\Gamma_j^{x_a,x_o}\right) = \sum_{F_i \in F} \mathcal{L}\left(\Gamma_{j_{|F_i}}^{x_a,x_o}\right) \tag{3}$$

where $\mathcal{L}\left(\Gamma_{j_{|F_i}}^{x_a,x_o}\right)$ is measured according to the euclidean distance. We define the shortest discrete geodesic Γ_G as the shortest path:

$$\Gamma_G = \underset{x_a,x_o,j}{\text{argmin}}\ \mathcal{L}\left(\Gamma_j^{x_a,x_o}\right) \tag{4}$$

The length $\mathcal{L}(\Gamma_G)$ results to be the shortest geodesic distance. We use the Dijkstra method (Lanthier, 2000; Dijkstra, 2022) to find the set of discrete geodesic over the entire aortic domain connecting all points $x_a \in \Omega_{annulus}$ with $x_o \in \Omega_{ostium}$ and we select the shortest of them. The resulting broken line is then smoothed to obtain the aortic internal curvature line (ICL).

Afterwards, for each section Ψ_k, defining x_{ic_k} the point of intersection between Ψ_k and *ICL*, the direction given by the versor $\overrightarrow{v_{c_k}}$ pointing towards the centre of the aorta x_{c_k} is identified:

$$\overrightarrow{v_{c_k}} = \frac{\overrightarrow{x_{ic_k} x_{c_k}}}{\left\| \overrightarrow{x_{ic_k} x_{c_k}} \right\|} \tag{5}$$

The intersection between the axis along the direction $\overrightarrow{v_{c_k}}$ and S defines a new point x_{ec_k} (**Figure 2C**). The repetition of this procedure on the n sections Ψ_k allows to create a spline corresponding to the external curvature line (*ECL*). In **Figure 2D**, *ECL* and *ICL* are shown. The ratio between the external and internal curvature line lengths *EILR* is then computed:

$$EILR = \frac{\mathcal{L}(ECL)}{\mathcal{L}(ICL)} \tag{6}$$

2.3.4 Tortuosity

The last local shape feature we compute is the tortuosity T, defined as:

$$T = \frac{\mathcal{L}(C)}{\mathcal{L}(C_0)} \tag{7}$$

where C_0 is the straight line connecting the first and the last points of C.

Except for the manual identification of the brachio-cephalic trunk ostium, the procedure for computing the shape features is without any user interaction. The geometric decomposition methods are developed using Python, VTK, ITK and Qt in 3DSlicer environment.

2.4 Growth rate evaluation

Even if the diameter threshold for elective surgery has not yet been reached, it is however clear that a patient with rapid AsAA growth over time should be carefully and constantly monitored (Geisbüsch et al., 2014). In this regard, we assume that the risk of aneurysm rupture is intrinsically derived from the risk of aneurysm growth (Coady et al., 1997; Saliba et al., 2015). Exploiting longitudinal data, the AsAA GR can be evaluated as ratio between the difference in maximum diameters and the time interval Δt in months between the two scans:

$$\mathrm{GR} = \frac{D'' - D'}{\Delta t} \tag{8}$$

where D' is the diameter D related to the first exam and D'' to the second acquisition. The Mann-Whitney test is used to compare the GR values derived from ECG-gated data with those computed on patients for whom at least one acquisition was not gated. The relationship between the proposed local shape features and the growth rate is then evaluated using Spearman's correlation coefficients. Statistical analysis is performed using Matlab (version 9.12.0, R2022a).

2.5 Machine learning classification

We divided the patients into two risk classes according to the observed growth rate. All patients with GR $\leq$ 0.25 mm/month composed the low-risk class (41 patients) while the others represented the group with rapid growth (9 patients). This threshold was chosen according to the surgery guidelines previously mentioned. For every individual, we then tried to predict the belonging class by using ML classifiers with in input the metrics derived from the first acquisition acting as possible predictors of growth. We initially tested the diameter D alone derived from the first exam in order to predict the GR-related risk class. Then, a second classification was conducted selecting all the shape features together. Six different classification models (Silva et al., 2019) were used: decision tree (DT) (Ali and Smith, 2006), linear discriminant (LD) (Duda et al., 2000), logistic regression (LR) (Dreiseitl and Ohno-Machado, 2002), naive bayes (Ren et al., 2009), support vector machine (SVM) (Cortes and Vapnik, 1995) and k-nearest neighbours (KNN) (Altman, 1992). Except for LR, the hyperparameter values were optimized minimizing the classification error. We use a leave-one-out cross-validation method to assess the predictive accuracy of the classification models. The accuracy is defined as:

$$\text{accuracy} = \frac{\mathrm{TP} + \mathrm{TN}}{\mathrm{TP} + \mathrm{TN} + \mathrm{FP} + \mathrm{FN}} \tag{9}$$

Sensitivity and specificity are calculated as:

$$\text{sensitivity} = \frac{\mathrm{TP}}{\mathrm{TP} + \mathrm{FN}} \tag{10}$$

$$\text{specificity} = \frac{\mathrm{TN}}{\mathrm{TN} + \mathrm{FP}} \tag{11}$$

where true positive (TP) is the number of fast-growing aortas correctly identified, true negative (TN) the number of low-risk shapes correctly identified, false negative (FN) the number of high-risk geometries incorrectly identified as low risk and false positive (FP) the number of low-risk shapes incorrectly identified as high risk. We obtained these values analyzing the confusion matrix, a 2 × 2 matrix where the diagonal represents the aortas that were correctly classified and the anti-diagonal represented misclassifications. In addition to accuracy, sensitivity and specificity, the performances were measured using the area under the receiver operating characteristic (AUROC) curve which represents the probability that the input parameter (parameters) is (are) higher for the class with fast growth than for the one with slow growth and thus, is a measure of discrimination. Finally, to describe the diagnostic value of the proposed shape features, likelihood ratios (LHRs) are used:

$$\mathrm{LHR}+ = \frac{\text{sensitivity}}{1 - \text{specificity}} \tag{12}$$

$$\mathrm{LHR}- = \frac{1 - \text{sensitivity}}{\text{specificity}} \tag{13}$$

LHR+ (LHR−) represents the change in the odds of having a diagnosis in patients with a positive (negative) test.

3 Results

The full dataset presented a mean follow-up of 31 ± 25 months. AAo segmentations were performed for all 100 acquisitions and the

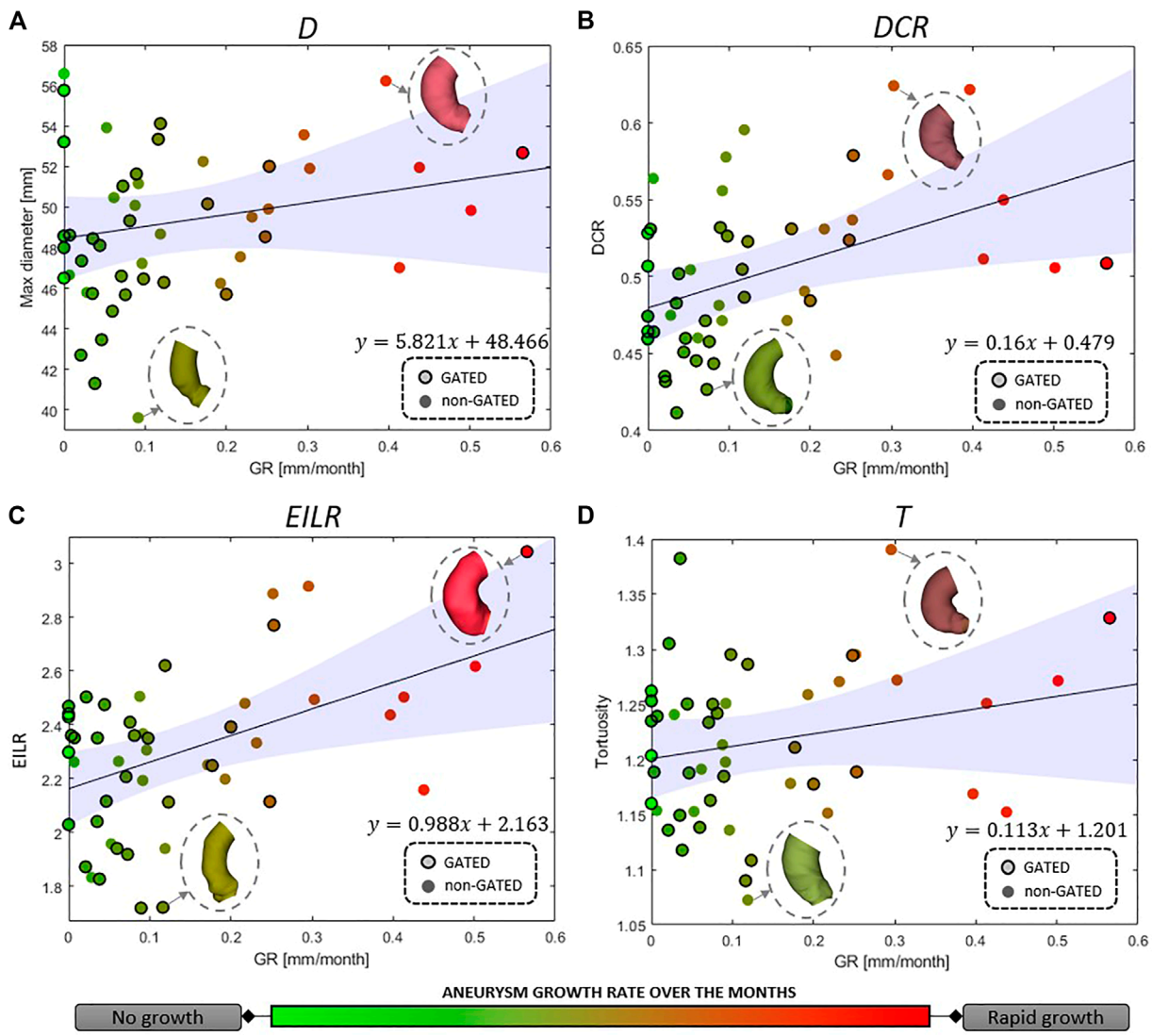

FIGURE 3
Correlation between growth rate and **(A)** maximum aneurysm diameter *D*, **(B)** ratio of maximum diameter and centerline length *DCR*, **(C)** ratio of external and internal curvature line length *EILR* and **(D)** tortuosity *T*. The circles around the marker edges indicate patients with two gated acquisitions in the same phase of the cardiac cycle. The line for linear correlation with 95% fitting confidence bounds is reported, the fitting equation provided and some of the AAo shapes shown.

shape metrics were extracted for the first exam of all patients. The median GR was 0.09 mm/month with an interquartile range IQR = 0.17 mm/month, in agreement with what reported in (Coady et al., 1999; Adriaans et al., 2021). The highest derived growth rate was 0.56 mm/month. The null hypothesis that GRs computed from ECG-gated and non-gated acquisitions can be attributable to a distribution with equal median was accepted ($p = 0.048$).

For the full set of patients, the values of the computed shape features, expressed as median (IQR), are the following: 48.64 mm (5.46 mm) for *D*, 0.50 (0.07) for *DCR*, 2.32 (0.35) for *EILR* and 1.21 (0.10) for *T*. In **Figure 3**, we report the relationship between the shape features and the growth rate: the colour of each marker provides an idea of the GR "intensity," from light green (no growth) to bright red (fast growth). A positive correlation is observed between GR and all four derived measurements. We obtain the following Spearman's coefficients: $r = 0.169$ ($p = 0.091$) for *D*, $r = 0.511$ ($p = 1.3e\text{-}4$) for *DCR*, $r = 0.472$ ($p = 2.7e\text{-}4$) for *EILR*, $r = 0.161$ ($p = 0.121$) for *T*. A statistically significant moderate correlation between *DCR* and GR and between *EILR* and GR is thus evident while the shape features *D* and *T* do not reach the significance p-level.

Concerning the classification, 9 patients (18% prevalence) were identified with growth rates above the threshold of 0.25 mm/month. The confusion matrices are reported in **Figure 4** both for the diameter alone as growth predictor and for the four shape features together. **Table 2** reports the performance of the six classifiers in terms of accuracy, sensitivity, specificity, LHR+ and LHR−. The AUROC for the six classifiers is shown in **Figure 5**. Using only *D* as risk class predictor, four of the classifiers (LD, LR, NB, and SVM) prove unable to identify high-risk patients (sensitivity = 0%).

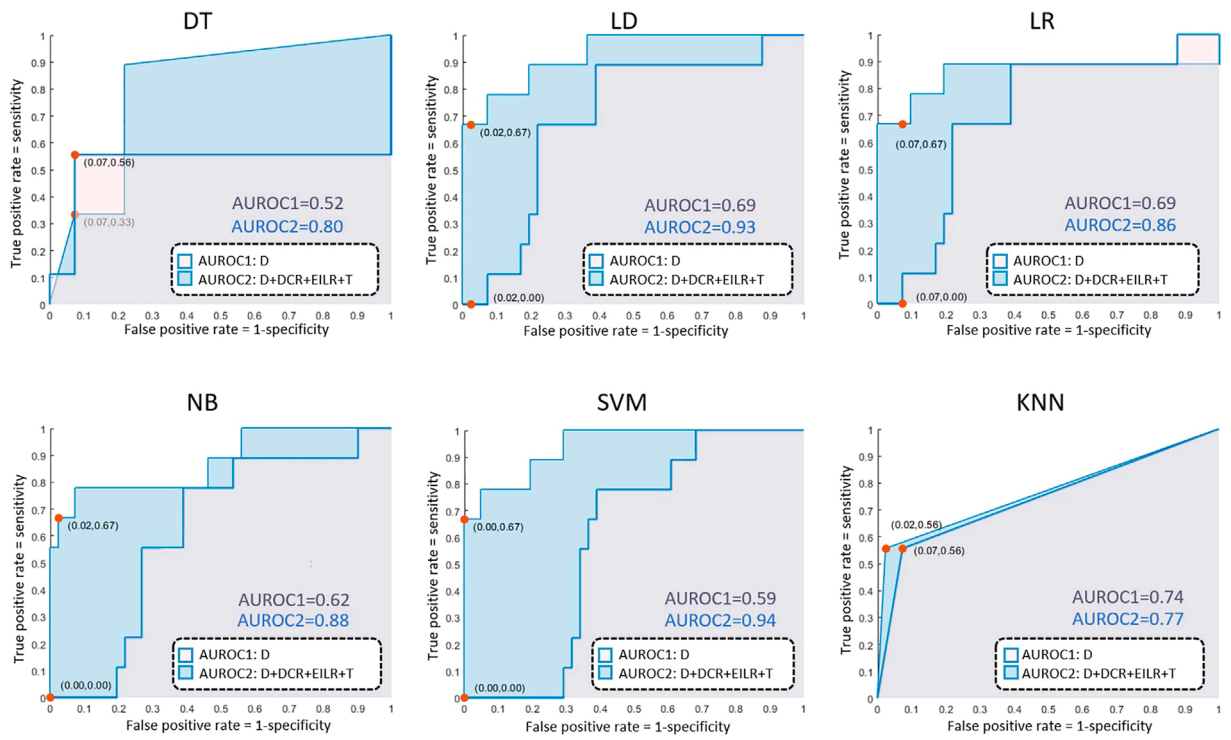

FIGURE 4
AUROC results for the decision tree (DT), linear discriminant (LD), logistic regression (LR), naive bayes (NB), support vector machine (SVM), k-nearest neighbours (KNN) classifiers.

TABLE 2 Classification scores for the six classifiers obtained with leave-one-out cross-validation: decision tree (DT), linear discriminant (LD), logistic regression (LR), naive bayes (NB), support vector machine (SVM) and k-nearest neighbours (KNN).

	DT	LD	LR	NB	SVM	KNN
Accuracy (*D*)	82%	80%	76%	82%	82%	**86%**
Accuracy (*D* + *DCR* + *EILR* + *T*)	86%	92%	88%	92%	**94%**	90%
Sensitivity (*D*)	33.3%	0%	0%	0%	0%	**55.6%**
Sensitivity (*D* + *DCR* + *EILR* + *T*)	55.6%	**66.7%**	**66.7%**	**66.7%**	**66.7%**	55.6%
Specificity (*D*)	92.7%	97.6%	92.7%	**100%**	**100%**	92.7%
Specificity (*D* + *DCR* + *EILR* + *T*)	92.7%	97.6%	92.7%	97.6%	**100%**	97.6%
LHR+ (*D*)	4.56	0	0	//	//	**7.62**
LHR+ (*D* + *DCR* + *EILR* + *T*)	7.62	27.79	9.13	27.79	+∞	23.17
LHR− (*D*)	0.72	1.02	1.08	1	1	**0.48**
LHR- (*D* + *DCR* + *EILR* + *T*)	0.48	0.34	0.36	0.34	**0.33**	0.45

The symbol // indicates undefined. Best performances are marked in bold.

Among the *D*-based classifiers, KNN reports the highest accuracy (86%), sensitivity (55.6%), AUROC (0.74), LHR+ (7.62) and the lower LHR− (0.48). Instead, the KNN specificity is 92.7%, lower than that resulting from LD (97.6%), NB (100%), SVM (100%) and equal to the values obtained through DT and LR. On the other side, considering the four shape features together, the best performances are obtained using SVM. It returns the highest accuracy (94%), sensitivity (66.7%), specificity (100%), AUROC (0.94) and LHR+ (tending to ∞). Even for LHR−, the best performance among the classifiers is achieved with a value of 0.33. In this case, DT is

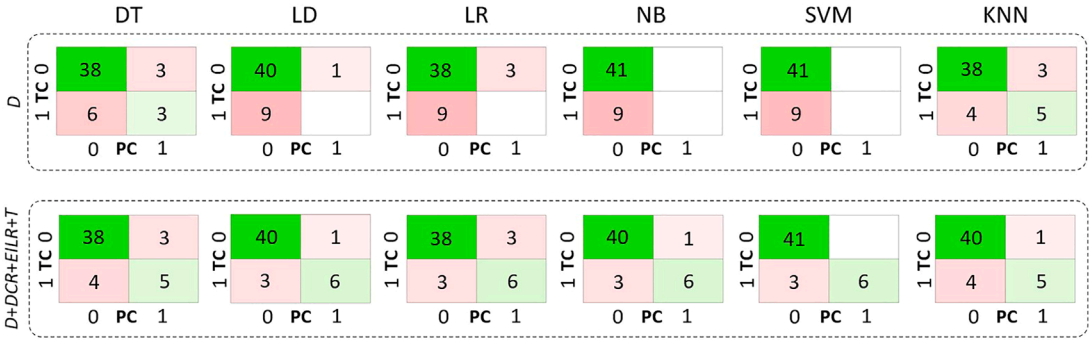

FIGURE 5
Confusion matrices related only to *D* on the first row and to *D*, *DCR*, *EILR* and *T* on the second row for the decision tree (DT), linear discriminant (LD), logistic regression (LR), naive bayes (NB), support vector machine (SVM), k-nearest neighbours (KNN) classifiers. TC means true class while PC means predicted class.

performing worse showing accuracy = 86%, sensitivity = 55.6%, specificity = 92.7%, LHR+ = 4.56, LHR− = 0.48 and AUROC = 0.52. **Figure 5** shows how the AUROC is always superior for the classifiers with the four shape parameters as input compared to the equivalent diameter-only based classifiers. This is also clear by analyzing **Table 2**, where all the values calculated for the classification with the four parameters are equal to or outperform those of the classification with the diameter alone, except for the NB classifier specificity.

4 Discussion

In this work, we present a method for computing four local shape features on the ascending aorta and we compare the ability to identify patients at high risk of aneurysm growth through six classifiers based on these local parameters with the same classifiers based on the maximum diameter alone. We observed how each ML classifier returns a more accurate risk prediction when using the four shape features together.

The patients used for the shape metrics computation were derived from gated and non-gated acquisitions. We included a temporal filtering criterion of 6 months between the first and the second exam to reduce the uncertainty of the results, especially for the GR assessment (De Heer et al., 2011; Zubair et al., 2020). Moreover, we decided not to consider in this study patients with Marfan syndrome or in general congenital degenerative wall diseases since they could affect the results given the rapid aneurysm growth they could exhibit. The uncertainty introduced by using both CT-Scans and MRI-Angiographies is however mitigated by considering the selected exclusion criteria and by deriving segmented geometries corresponding to the intra-luminal regions from both types of acquisition. Minor and non-significant differences were indeed described when comparing diameters obtained from these two imaging techniques (Bons et al., 2019; Frazao et al., 2020).

After the segmentation and identification of the ascending aorta, the computation of shape metrics is performed on the entire AAo domain, including the Valsalva sinuses. This enables even aneurysms of the root region to be investigated. *D* is the only quantity that provides non-normalized local information with respect to the shape of the aorta. *DCR* returns a measurement of diameter in relation to a local length, which allows a better understanding of the differences between tall and robust patients and more slender individuals. *EILR*, on the other hand, gives information on the relationship between the external and the internal curvature line, to be carefully considered in the case of wall expansion toward the external direction of the aorta, as in saccular or root aneurysm (David, 2010). Finally, *T* returns another important piece of information, different from the previous ones, on how contorted and twisted the AAo is. Additional parameters such as volume and surface area of the ascending tract were not included as they were considered characteristic measures of vessel size and not shape (Heuts et al., 2020).

We evaluate the growth rate as the difference between the maximum diameters derived from two exams, normalized by the distance in months between the two. This is, of course, a simplification since it seems that the aneurysm evolution follows an exponential law over time rather than a linear one (Hirose et al., 1995). In fact, according to Laplace's law, wall tension is proportional to the vessel radius for a given blood pressure. So, growth rates become higher as the aorta progressively enlarges. Several empirical models have been presented to account for exponential growth rates exploiting multiple time exams (Gharahi et al., 2015). Information on how and whether aortic dilatation is accelerating over time could in fact further improve the prediction results. However, as most of the patients in the group had only two acquisitions and an exponential growth rate laws usually require controls over at least three different time instants for their validation (Martufi et al., 2013), the linear model was preferred. Additionally, in this study, D'' and D' can be at different centerline levels. Obviously, obtaining the maximum diameter at a certain distance from the annulus for the first exam and evaluating the diameter from the model related to the second acquisition using the same distance, without a new search for the maximum along the centerline, would produce different results in terms of GR with values that would certainly be lower or at most equal to those we used. As reflected in the data subdivision, only 9 (18%) patients showed a rapid evolution. This majority of patients with slow-growing aneurysms probably derives from the fact that the clinicians themselves, after a first

3-dimensional acquisition, often decide to make a second acquisition some months later when, based on clinical data, they suppose the disease will not evolve quickly and the dilatation phenomenon will not be abrupt and dangerous. It is worth noting that there are only 3 (6%) patients with the maximum diameter over 55 mm on whom local metrics were computed and two of these show a close to zero growth rate. We suppose they had not been surgically treated due to a precarious health state or because manual measurements of the diameter returned values below the threshold for surgery, really close to the value we measured. This, together with a correlation that is not strong neither statistically significant, are the reasons why classification based only on *D* results in failure. The performances of the individual diameter-based classifiers are, in fact, fairly low. This suggests that the diameter alone, current criterion for rupture risk, fails to accurately predict the growth, at least with respect to the data we collected. KNN, being based on the vote derived from the neighbouring classes, is the unique classifier able to discriminate at least 5 of the 9 patients of the high-GR risk class. Integrating the four features together and using the same KNN, a performance improvement (**Table 2**) is appreciable. However, among the classifiers based on all metrics, the best results are obtained using SVM. Although the sensitivity of SVM, i.e., the correct prediction rate for high-risk patients, never exceeds the 66.7% threshold, its accuracy, LHR+ and LHR− make it a good candidate in terms of utility (Ranganathan and Aggarwal, 2018). LHR + tending to $+\infty$ indicates that in case of a positive result, a patient definitely belongs to the high-risk group. LHR− = 0.33 means that a person on which a GR under the threshold is identified is about 3 (=1/0.33) times more likely to have a negative test than someone with a GR over the threshold. Since LHR+ and LHR− do not depend on the prevalence value, they are considered robust measures of the diagnostic capacity of the proposed classifiers. As reported in (Ray et al., 2010), an excellent classification method would return a LHR + higher than 10 and a LHR− lower than 0.1. Unfortunately, SVM fails to reach the threshold related to LHR−. However, we are confident that adding new parameters such as patient age, aortic valve type and possible related diseases, hypertension status or numerical simulation results (Groth et al., 2018; Biancolini et al., 2020) may improve the classification performances in that direction. Maier et al. (2010) have indeed proved how numerical simulation results as the stress at the wall and the ratio of wall stress and strength could be used to improve the prediction of abdominal aortic aneurysm rupture. The integration of this information may help to reduce the misclassifications that occur when using the shape features alone. Moreover, including detailed patient-specific material properties (Reeps et al., 2013) and an estimation of the geometry related to the stress-free state (Gee et al., 2009) could allow for even more accurate risk assessments. In any case, this is beyond the scope of this work, which concerns only the analysis of local parameters related to the ascending aorta shape. The presence of FNs in this type of classification is one of the most delicate aspects as it could lead to patients whose pathology is evolving quickly not being treated beforehand. In this regard, we consider interesting to observe the geometries related to the three patients classified as FNs from SVM for the full set of shape features, whose complete segmentations are shown in **Figure 6**. Two of them exhibit aortic coarctation (the only ones in the dataset) while one has an abrupt change between aortic arch and descending aorta with a very small radius of curvature. These morphological anomalies, altering the pressure gradient, obviously affect the fluid dynamics of the ascending aorta (Oliver et al., 2009). This could be the reason why, although the shape features of the ascending tract are not such as to characterize the patient as being at high risk, the disease undergoes a severe and rapid evolution over time. Four shape features alone are obviously not sufficient to predict the aneurysm growth but the results of this work clearly indicate the importance of considering the shape in studying the evolution of the pathology. Certainly, the AsAA surgical repair decision cannot derive exclusively from the analysis of the AAo alone but requires an integration of information from the upstream region (aortic valve) and the downstream part (arch and descending section). We also stress that the use of diameter as a criterion for surgery should not be replaced by these new features, but rather complemented by them since they, valuable in improving the assessment of the risk of growth, have not yet been proven effective in predicting the rupture. Overall, machine learning methods prove to be excellent candidates for improving the prediction of ascending aortic aneurysm shapes prone to rapid growth (Hahn et al., 2021) and delivering more personalized control and treatment plans (Monsalve-Torra et al., 2016). They are particularly suitable for integrating large amounts of data, including patient demographics, lifestyle factors, clinical history and medical images (Ashkezari et al., 2022). Moreover, ML algorithms can be used to track shape modifications in time and provide dynamic predictions of aortic aneurysm growth (Jiang et al., 2020), allowing for timely intervention. Unfortunately, multiple 3D longitudinal data are generally available for a limited number of patients and therefore a robust validation of the predictive ability is still challenging. Although this work shows that linking shape features derived from longitudinal data and ML classifiers is a promising approach to predict the aneurysm growth, some limitations need to be mentioned. The most important are the small dataset of patients used and the unequal distribution of classes. A more accurate study must necessarily include a larger number of patients with ECG-gated acquisitions performed at high resolution. A robust automatic segmentation method that removes manual correction processes would then be required, thus avoiding any bias introduced by the operator (Ashok and Gupta, 2021). Moreover, the uncertainty of the results is not only due to the segmentation task but also to the delimitation of the ascending aorta domain. Some of the patients were probably treated between one acquisition and the following with drugs such as beta-blockers that definitely affected the growth of the vessel over the months thus altering the correlation results between shape features and GR. It should also be mentioned that, as this study was exclusively related to the shape, we did not consider other important features such as material properties of the aorta wall and vessel thickness (Lin et al., 2022) which could further improve the results in terms of accuracy. The shape features described here relate exclusively to local properties. Future work will incorporate global shape features given by the modes of a statistical shape model (SSM) (Zheng et al., 2017) that will likely improve the model prediction. Although Cosentino et al. (2020) showed that, especially for the first principal modes, there is not a significant difference in terms of AAo wall shape between patients with bicuspid and tricuspid aortic valve, a subdivision into two different subsets would produce better results in terms of accuracy (Rooprai et al., 2019). Lastly, as previously introduced, it would

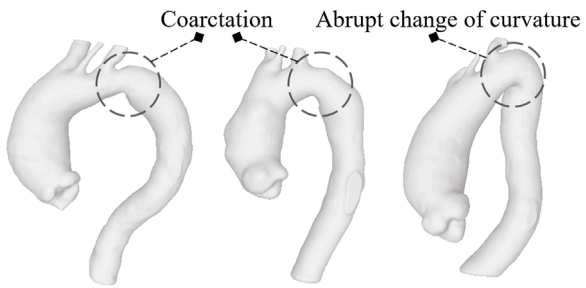

FIGURE 6
The models classified as FNs by SVM based on the four shapes features: the first two report aortic coarctation while the third shows a reduced radius of curvature between the arch and descending aorta.

also be interesting to assign a risk score to the valve type, to the possible level of calcification and to other co-existing risk factors and observe how the classification results would change according to them. A more in-depth analysis of the aortic valve would be consequently required although it is not straightforward to derive such information for all patients from this retrospective dataset. After further validations of the predictive capabilities through large-scale studies by including these multiple factors and overcoming the limitations described before, the reliability of these methods in clinical environments could be definitively established.

5 Conclusion

In this paper, we explain how to compute some shape features useful for classifying patients at high risk of rapid AsAA evolution. By using ML classifiers based on data derived from 50 patients, this work provides an indication that a set of AsAA local features could help in classifying the aneurysm growth potential more accurately than the maximum diameter alone. By treating large amounts of data, handling complex relationships and offering personalized predictions, machine learning can enhance the management and treatment of this dangerous disease. Deepening this combination of non-invasive geometric quantification and statistical machine learning methods and integrating these results with those derived from the numerical simulation could help in identifying aortic shapes potentially at risk of aneurysm growth and could certainly be useful not only for surgery planning but also for both the choice of therapy and the follow-up timing. In fact, this work might be important in a clinical environment to assess the risk of rupture of aneurysms during regular patient follow-up and might allow the development of personalized decision-making processes that will take into account not only the aneurysm shape but also several additional patient-specific data. The new shape features proposed here should not replace the diameter itself but complement it in order to have a more detailed understanding of this complex biological problem. It is obvious, therefore, that in order to consider these shape parameters as real biomarkers related to the AsAA evolution, the predictive capacity needs to be further strengthened by identifying and preparing a larger prospective study.

Data availability statement

The original contributions presented in the study are included in the article/supplementary materials, further inquiries can be directed to the corresponding author.

Ethics statement

The studies involving human participants were reviewed and approved by Cardiac and Vascular Thoracic Surgery at Rennes University Hospital, France. Cardivascular and Thoracic Surgery at Dijon University Hospital, France. Cardiac Surgery at Toulouse University Hospital, France. Written informed consent for participation was not required for this study in accordance with the national legislation and the institutional requirements.

Author contributions

LG: data preparation, data analysis, methodology, software, writing; PH: methodology, conceptualization, revision, AM: data preparation, methodology, software, revision; KY: data preparation; MR: resources, supervision; AB-B: methodology, revision; SL: data search, revision; DM-C: data collection; AL; methodology, revision; OB: methodology; MD: data collection, methodology; PE: data collection, methodology; JT: data collection, methodology, conceptualization; JP: data collection; PPV: conceptualization, review; MEB: resources, supervision, review. All authors contributed to the article and approved the current version of the manuscript.

Funding

The research has received funding from the European Union's Horizon 2020 research and innovation programme under the Marie Skłodowska-Curie grant agreement No 859836, MeDiTATe: "The Medical Digital Twin for Aneurysm Prevention and Treatment".

Conflict of interest

Authors LG, AM, KY, and MR were employed by Ansys France.

The remaining authors declare that the research was conducted in the absence of any commercial or financial relationships that could be construed as a potential conflict of interest.

Publisher's note

All claims expressed in this article are solely those of the authors and do not necessarily represent those of their affiliated organizations, or those of the publisher, the editors and the reviewers. Any product that may be evaluated in this article, or claim that may be made by its manufacturer, is not guaranteed or endorsed by the publisher.

References

Adriaans, B., Ramaekers, M., Heuts, S., Crijns, H., Bekkers, S., Westenberg, J., et al. (2021). Determining the optimal interval for imaging surveillance of ascending aortic aneurysms. *Neth. Heart J.* 29, 623–631. doi:10.1007/s12471-021-01564-9

Ali, S., and Smith, K. A. (2006). On learning algorithm selection for classification. *Appl. Soft Comput.* 6, 119–138. doi:10.1016/j.asoc.2004.12.002

Altman, N. S. (1992). An introduction to kernel and nearest-neighbor nonparametric regression. *Am. Stat.* 46, 175–185. doi:10.2307/2685209

Anfinogenova, N. D., Sinitsyn, V. E., Kozlov, B. N., Panfilov, D. S., Popov, S. V., Vrublevsky, A. V., et al. (2022). Existing and emerging approaches to risk assessment in patients with ascending thoracic aortic dilatation. *J. Imaging* 8, 280. doi:10.3390/jimaging8100280

Ashkezari, S. S., Mut, F., Slawski, M., Jimenez, C., Robertson, A., and Cebral, J. (2022). Identification of small, regularly shaped cerebral aneurysms prone to rupture. *Am. J. Neuroradiol.* 43, 547–553. doi:10.3174/ajnr.A7470

Ashok, M., and Gupta, A. (2021). A systematic review of the techniques for the automatic segmentation of organs-at-risk in thoracic computed tomography images. *Arch. Comput. Methods Eng.* 28, 3245–3267. doi:10.1007/s11831-020-09497-z

Biancolini, M. E., Capellini, K., Costa, E., Groth, C., and Celi, S. (2020). Fast interactive cfd evaluation of hemodynamics assisted by rbf mesh morphing and reduced order models: The case of ataa modelling. *Int. J. Interact. Des. Manuf.* 14, 1227–1238. doi:10.1007/s12008-020-00694-5

Bons, L. R., Duijnhouwer, A. L., Boccalini, S., van den Hoven, A. T., van der Vlugt, M. J., Chelu, R. G., et al. (2019). Intermodality variation of aortic dimensions: How, where and when to measure the ascending aorta. *Int. J. Cardiol.* 276, 230–235. doi:10.1016/j.ijcard.2018.08.067

Califf, R. M. (2018). Biomarker definitions and their applications. *Exp. Biol. Med.* 243, 213–221. doi:10.1177/1535370217750088

Coady, M. A., Rizzo, J. A., Hammond, G. L., Mandapati, D., Darr, U., Kopf, G. S., et al. (1997). What is the appropriate size criterion for resection of thoracic aortic aneurysms? *J. Thorac. Cardiovasc. Surg.* 113, 476–491. doi:10.1016/S0022-5223(97)70360-X

Coady, M. A., Rizzo, J. A., Hammond, G. L., Kopf, G. S., and Elefteriades, J. A. (1999). Surgical intervention criteria for thoracic aortic aneurysms: A study of growth rates and complications. *Ann. Thorac. Surg.* 67, 1922–1926. doi:10.1016/s0003-4975(99)00431-2

Cortes, C., and Vapnik, V. (1995). Support-vector networks. *Mach. Learn.* 20, 273–297. doi:10.1007/bf00994018

Cosentino, F., Raffa, G. M., Gentile, G., Agnese, V., Bellavia, D., Pilato, M., et al. (2020). Statistical shape analysis of ascending thoracic aortic aneurysm: Correlation between shape and biomechanical descriptors. *J. Pers. Med.* 10, 28. doi:10.3390/jpm10020028

David, T. E. (2010). Surgical treatment of ascending aorta and aortic root aneurysms. *Prog. Cardiovasc. Dis.* 52, 438–444. doi:10.1016/j.pcad.2009.12.005

Davies, R. R., Kaple, R. K., Mandapati, D., Gallo, A., Botta, D. M. Jr, Elefteriades, J. A., et al. (2007). Natural history of ascending aortic aneurysms in the setting of an unreplaced bicuspid aortic valve. *Ann. Thorac. Surg.* 83, 1338–1344. doi:10.1016/j.athoracsur.2006.10.074

De Heer, L. M., Budde, R. P., Mali, W. P. T. M., de Vos, A. M., van Herwerden, L. A., and Kluin, J. (2011). Aortic root dimension changes during systole and diastole: Evaluation with ecg-gated multidetector row computed tomography. *Int. J. Cardiovasc. Imaging* 27, 1195–1204. doi:10.1007/s10554-011-9838-x

Dey, T. K., and Zhao, W. (2002). "Approximate medial axis as a voronoi subcomplex," in Proceedings of the seventh ACM symposium on Solid modeling and applications, 356–366.

Dijkstra, E. W. (2022). "A note on two problems in connexion with graphs," in *Edsger wybe Dijkstra: His life, work, and legacy* (Association for Computing Machinery), 287–290.

Doyle, B. J., Callanan, A., Burke, P. E., Grace, P. A., Walsh, M. T., Vorp, D. A., et al. (2009). Vessel asymmetry as an additional diagnostic tool in the assessment of abdominal aortic aneurysms. *J. Vasc. Surg.* 49, 443–454. doi:10.1016/j.jvs.2008.08.064

Dreiseitl, S., and Ohno-Machado, L. (2002). Logistic regression and artificial neural network classification models: A methodology review. *J. Biomed. Inf.* 35, 352–359. doi:10.1016/s1532-0464(03)00034-0

Duda, R. O., Hart, P. E., and Stork, D. G. (1973). *Pattern classification and scene analysis* 3. New York: Wiley.

Elefteriades, J. A., and Farkas, E. A. (2010). Thoracic aortic aneurysm: Clinically pertinent controversies and uncertainties. *J. Am. Coll. Cardiol.* 55, 841–857. doi:10.1016/j.jacc.2009.08.084

Fedorov, A., Beichel, R., Kalpathy-Cramer, J., Finet, J., Fillion-Robin, J.-C., Pujol, S., et al. (2012). 3d slicer as an image computing platform for the quantitative imaging network. *Magn. Reson. Imaging* 30, 1323–1341. doi:10.1016/j.mri.2012.05.001

Frazao, C., Tavoosi, A., Wintersperger, B. J., Nguyen, E. T., Wald, R. M., Ouzounian, M., et al. (2020). Multimodality assessment of thoracic aortic dimensions: Comparison of computed tomography angiography, magnetic resonance imaging, and echocardiography measurements. *J. Thorac. Imaging* 35, 399–406. doi:10.1097/RTI.0000000000000514

Gee, M., Reeps, C., Eckstein, H., and Wall, W. (2009). Prestressing in finite deformation abdominal aortic aneurysm simulation. *J. Biomech.* 42, 1732–1739. doi:10.1016/j.jbiomech.2009.04.016

Geisbüsch, S., Stefanovic, A., Schray, D., Oyfe, I., Lin, H.-M., Di Luozzo, G., et al. (2014). A prospective study of growth and rupture risk of small-to-moderate size ascending aortic aneurysms. *J. Thorac. Cardiovasc. Surg.* 147, 68–74. doi:10.1016/j.jtcvs.2013.06.030

Gharahi, H., Zambrano, B., Lim, C., Choi, J., Lee, W., and Baek, S. (2015). On growth measurements of abdominal aortic aneurysms using maximally inscribed spheres. *Med. Eng. Phys.* 37, 683–691. doi:10.1016/j.medengphy.2015.04.011

Grobman, W. A., and Stamilio, D. M. (2006). Methods of clinical prediction. *Am. J. Obstet. Gynecol.* 194, 888–894. doi:10.1016/j.ajog.2005.09.002

Groth, C., Porziani, S., Biancolini, M., Costa, E., Celi, S., Capellini, K., et al. (2018). The medical digital twin assisted by reduced order models and mesh morphing. In International CAE Conference. 10

Guo, M. H., Appoo, J. J., Saczkowski, R., Smith, H. N., Ouzounian, M., Gregory, A. J., et al. (2018). Association of mortality and acute aortic events with ascending aortic aneurysm: A systematic review and meta-analysis. *JAMA Netw. Open* 1, e181281. doi:10.1001/jamanetworkopen.2018.1281

Hahn, L. D., Baeumler, K., and Hsiao, A. (2021). Artificial intelligence and machine learning in aortic disease. *Curr. Opin. Cardiol.* 36, 695–703. doi:10.1097/HCO.0000000000000903

Heuts, S., Adriaans, B. P., Rylski, B., Mihl, C., Bekkers, S. C., Olsthoorn, J. R., et al. (2020). Evaluating the diagnostic accuracy of maximal aortic diameter, length and volume for prediction of aortic dissection. *Heart* 106, 892–897. doi:10.1136/heartjnl-2019-316251

Hirose, Y., Hamada, S., and Takamiya, M. (1995). Predicting the growth of aortic aneurysms: A comparison of linear vs exponential models. *Angiology* 46, 413–419. doi:10.1177/000331979504600508

Jiang, Z., Do, H. N., Choi, J., Lee, W., and Baek, S. (2020). A deep learning approach to predict abdominal aortic aneurysm expansion using longitudinal data. *Front. Phys.* 7, 235. doi:10.3389/fphy.2019.00235

Kim, S., Jiang, Z., Zambrano, B. A., Jang, Y., Baek, S., Yoo, S. K., et al. (2022). Deep learning on multiphysical features and hemodynamic modeling for abdominal aortic aneurysm growth prediction. *IEEE Trans. Med. Imaging* 42, 196–208. doi:10.1109/TMI.2022.3206142

Krüger, T., Forkavets, O., Veseli, K., Lausberg, H., Vöhringer, L., Schneider, W., et al. (2016). Ascending aortic elongation and the risk of dissection. *Eur. J. Cardio-Thoracic Surg.* 50, 241–247. doi:10.1093/ejcts/ezw025

Krüger, T., Sandoval Boburg, R., Lescan, M., Oikonomou, A., Schneider, W., Vöhringer, L., et al. (2018). Aortic elongation in aortic aneurysm and dissection: The tübingen aortic pathoanatomy (taipan) project. *Eur. J. Cardio-Thoracic Surg.* 54, 26–33. doi:10.1093/ejcts/ezx503

Kuzmik, G. A., Sang, A. X., and Elefteriades, J. A. (2012). Natural history of thoracic aortic aneurysms. *J. Vasc. Surg.* 56, 565–571. doi:10.1016/j.jvs.2012.04.053

Lanthier, M. (2000). *Shortest path problems on polyhedral surfaces*. Ph.D. thesis. Ottawa, Canada: Carleton University.

Lee, K., Zhu, J., Shum, J., Zhang, Y., Muluk, S. C., Chandra, A., et al. (2013). Surface curvature as a classifier of abdominal aortic aneurysms: A comparative analysis. *Ann. Biomed. Eng.* 41, 562–576. doi:10.1007/s10439-012-0691-4

Liang, L., Liu, M., Martin, C., Elefteriades, J. A., and Sun, W. (2017). A machine learning approach to investigate the relationship between shape features and numerically predicted risk of ascending aortic aneurysm. *Biomechanics Model. Mechanobiol.* 16, 1519–1533. doi:10.1007/s10237-017-0903-9

Lin, S., Morgant, M. C., Marín-Castrillón, D. M., Walker, P. M., Glélé, L. S. A., Boucher, A., et al. (2022). Aortic local biomechanical properties in ascending aortic aneurysms. *Acta Biomater.* 149, 40–50. doi:10.1016/j.actbio.2022.06.019

Lindquist Liljeqvist, M., Bogdanovic, M., Siika, A., Gasser, T. C., Hultgren, R., and Roy, J. (2021). Geometric and biomechanical modeling aided by machine learning improves the prediction of growth and rupture of small abdominal aortic aneurysms. *Sci. Rep.* 11, 18040–18110. doi:10.1038/s41598-021-96512-3

Maier, A., Gee, M., Reeps, C., Pongratz, J., Eckstein, H.-H., and Wall, W. (2010). A comparison of diameter, wall stress, and rupture potential index for abdominal aortic aneurysm rupture risk prediction. *Ann. Biomed. Eng.* 38, 3124–3134. doi:10.1007/s10439-010-0067-6

Martufi, G., Auer, M., Roy, J., Swedenborg, J., Sakalihasan, N., Panuccio, G., et al. (2013). Multidimensional growth measurements of abdominal aortic aneurysms. *J. Vasc. Surg.* 58, 748–755. doi:10.1016/j.jvs.2012.11.070

Melo, R. G. E., Duarte, G. S., Lopes, A., Alves, M., Caldeira, D., e Fernandes, R. F., et al. (2021). "Incidence and prevalence of thoracic aortic aneurysms: A systematic review and meta-analysis of population-based studies," in *Seminars in thoracic and cardiovascular surgery* (Elsevier).

Members, T. F., Erbel, R., Aboyans, V., Boileau, C., Bossone, E., Bartolomeo, R. D., et al. (2014). 2014 esc guidelines on the diagnosis and treatment of aortic diseases: Document covering acute and chronic aortic diseases of the thoracic and abdominal aorta of the adult the task force for the diagnosis and treatment of aortic diseases of the European society of cardiology (esc). *Eur. heart J.* 35, 2873–2926. doi:10.1093/eurheartj/ehu281

Monsalve-Torra, A., Ruiz-Fernandez, D., Marin-Alonso, O., Soriano-Payá, A., Camacho-Mackenzie, J., and Carreño-Jaimes, M. (2016). Using machine learning methods for predicting inhospital mortality in patients undergoing open repair of abdominal aortic aneurysm. *J. Biomed. Inf.* 62, 195–201. doi:10.1016/j.jbi.2016.07.007

Oladokun, D., Patterson, B., Sobocinski, J., Karthikesalingam, A., Loftus, I., Thompson, M., et al. (2016). Systematic review of the growth rates and influencing factors in thoracic aortic aneurysms. *Eur. J. Vasc. Endovasc. Surg.* 51, 674–681. doi:10.1016/j.ejvs.2016.01.017

Oliver, J. M., Alonso-Gonzalez, R., Gonzalez, A. E., Gallego, P., Sanchez-Recalde, A., Cuesta, E., et al. (2009). Risk of aortic root or ascending aorta complications in patients with bicuspid aortic valve with and without coarctation of the aorta. *Am. J. Cardiol.* 104, 1001–1006. doi:10.1016/j.amjcard.2009.05.045

Papagiannis, J. (2017). Sudden death due to aortic pathology. *Cardiol. Young* 27, S36–S42. doi:10.1017/S1047951116002213

Pappu, S., Dardik, A., Tagare, H., and Gusberg, R. J. (2008). Beyond fusiform and saccular: A novel quantitative tortuosity index may help classify aneurysm shape and predict aneurysm rupture potential. *Ann. Vasc. Surg.* 22, 88–97. doi:10.1016/j.avsg.2007.09.004

Piccinelli, M., Veneziani, A., Steinman, D. A., Remuzzi, A., and Antiga, L. (2009). A framework for geometric analysis of vascular structures: Application to cerebral aneurysms. *IEEE Trans. Med. Imaging* 28, 1141–1155. doi:10.1109/TMI.2009.2021652

Poullis, M. P., Warwick, R., Oo, A., and Poole, R. J. (2008). Ascending aortic curvature as an independent risk factor for type a dissection, and ascending aortic aneurysm formation: A mathematical model. *Eur. J. Cardio-Thoracic Surg.* 33, 995–1001. doi:10.1016/j.ejcts.2008.02.029

Pyeritz, R. E., and McKusick, V. A. (1979). The marfan syndrome: Diagnosis and management. *N. Engl. J. Med.* 300, 772–777. doi:10.1056/NEJM197904053001406

Radl, L., Jin, Y., Pepe, A., Li, J., Gsaxner, C., Zhao, F.-h., et al. (2022). Avt: Multicenter aortic vessel tree cta dataset collection with ground truth segmentation masks. *Data Brief* 40, 107801. doi:10.1016/j.dib.2022.107801

Ranganathan, P., and Aggarwal, R. (2018). Understanding the properties of diagnostic tests–part 2: Likelihood ratios. *Perspect. Clin. Res.* 9, 99–102. doi:10.4103/picr.PICR_41_18

Ray, P., Manach, Y. L., Riou, B., Houle, T. T., and Warner, D. S. (2010). Statistical evaluation of a biomarker. *J. Am. Soc. Anesthesiol.* 112, 1023–1040. doi:10.1097/ALN.0b013e3181d47604

Reeps, C., Maier, A., Pelisek, J., Härtl, F., Grabher-Meier, V., Wall, W., et al. (2013). Measuring and modeling patient-specific distributions of material properties in abdominal aortic aneurysm wall. *Biomech. Model. Mechanobiol.* 12, 717–733. doi:10.1007/s10237-012-0436-1

Ren, J., Lee, S. D., Chen, X., Kao, B., Cheng, R., and Cheung, D. (2009). "Naive bayes classification of uncertain data," in 2009 Ninth IEEE international conference on data mining (IEEE), 944–949.

Rengarajan, B., Wu, W., Wiedner, C., Ko, D., Muluk, S. C., Eskandari, M. K., et al. (2020). A comparative classification analysis of abdominal aortic aneurysms by machine learning algorithms. *Ann. Biomed. Eng.* 48, 1419–1429. doi:10.1007/s10439-020-02461-9

Rooprai, J., Boodhwani, M., Beauchesne, L., Chan, K.-L., Dennie, C., Nagpal, S., et al. (2019). Thoracic aortic aneurysm growth in bicuspid aortic valve patients: Role of aortic stiffness and pulsatile hemodynamics. *J. Am. Heart Assoc.* 8, e010885. doi:10.1161/JAHA.118.010885

Saeyeldin, A., Zafar, M. A., Li, Y., Tanweer, M., Abdelbaky, M., Gryaznov, A., et al. (2019). Decision-making algorithm for ascending aortic aneurysm: Effectiveness in clinical application? *J. Thorac. Cardiovasc. Surg.* 157, 1733–1745. doi:10.1016/j.jtcvs.2018.09.124

Saitta, S., Sturla, F., Caimi, A., Riva, A., Palumbo, M. C., Nano, G., et al. (2022). A deep learning-based and fully automated pipeline for thoracic aorta geometric analysis and planning for endovascular repair from computed tomography. *J. Digital Imaging* 35, 226–239. doi:10.1007/s10278-021-00535-1

Saliba, E., Sia, Y., Dore, A., and El Hamamsy, I. (2015). The ascending aortic aneurysm: When to intervene? *IJC Heart Vasc.* 6, 91–100. doi:10.1016/j.ijcha.2015.01.009

Schroeder, W., Maynard, R., and Geveci, B. (2015). "Flying edges: A high-performance scalable isocontouring algorithm," in 2015 IEEE 5th Symposium on Large Data Analysis and Visualization (LDAV), (IEEE), 33–40.

Senthilkumaran, N., and Vaithegi, S. (2016). Image segmentation by using thresholding techniques for medical images. *Comput. Sci. Eng. Int. J.* 6, 1–13. doi:10.5121/cseij.2016.6101

Shum, J., Martufi, G., Di Martino, E., Washington, C. B., Grisafi, J., Muluk, S. C., et al. (2011). Quantitative assessment of abdominal aortic aneurysm geometry. *Ann. Biomed. Eng.* 39, 277–286. doi:10.1007/s10439-010-0175-3

Silva, M. A., Patel, J., Kavouridis, V., Gallerani, T., Beers, A., Chang, K., et al. (2019). Machine learning models can detect aneurysm rupture and identify clinical features associated with rupture. *World Neurosurg.* 131, e46–e51. doi:10.1016/j.wneu.2019.06.231

Smoljkić, M., Fehervary, H., Van den Bergh, P., Jorge-Peñas, A., Kluyskens, L., Dymarkowski, S., et al. (2017). Biomechanical characterization of ascending aortic aneurysms. *Biomech. Model. Mechanobiol.* 16, 705–720. doi:10.1007/s10237-016-0848-4

Sonsino, A., Ellauzi, H., Ziganshin, B. A., Zafar, M. A., and Elefteriades, J. A. (2022). Rapid growth of thoracic aortic aneurysm: Reality or myth? *J. Thorac. Cardiovasc. Surg.* doi:10.1016/j.jtcvs.2022.06.021

Sweeting, M., and Thompson, S. (2012). Making predictions from complex longitudinal data, with application to planning monitoring intervals in a national screening programme. *J. R. Stat. Soc. Ser. A (Statistics Soc.)* 175, 569–586. doi:10.1111/j.1467-985X.2011.01005.x

Tozzi, P., Gunga, Z., Niclauss, L., Delay, D., Roumy, A., Pfister, R., et al. (2021). Type a aortic dissection in aneurysms having modelled pre-dissection maximum diameter below 45 mm: Should we implement current guidelines to improve the survival benefit of prophylactic surgery? *Eur. J. Cardio-Thoracic Surg.* 59, 473–478. doi:10.1093/ejcts/ezaa351

WSCG (2003). *The 11-th International Conference in Central Europe on Computer Graphics, Visualization and Computer Vision 2003*. Plzen, 13–16. ISBN: 80-903100-2-8

Wu, J., Zafar, M. A., Li, Y., Saeyeldin, A., Huang, Y., Zhao, R., et al. (2019). Ascending aortic length and risk of aortic adverse events: The neglected dimension. *J. Am. Coll. Cardiol.* 74, 1883–1894. doi:10.1016/j.jacc.2019.07.078

Zafar, M. A., Li, Y., Rizzo, J. A., Charilaou, P., Saeyeldin, A., Velasquez, C. A., et al. (2018). Height alone, rather than body surface area, suffices for risk estimation in ascending aortic aneurysm. *J. Thorac. Cardiovasc. Surg.* 155, 1938–1950. doi:10.1016/j.jtcvs.2017.10.140

Zheng, G., Li, S., and Szekely, G. (2017). *Statistical shape and deformation analysis: Methods, implementation and applications*. Cambridge, MA, United States: Academic Press.

Zubair, M. M., de Beaufort, H. W., Belvroy, V. M., Schwein, A., Irshad, A., Mohamed, A., et al. (2020). Impact of cardiac cycle on thoracic aortic geometry—Morphometric analysis of ecg gated computed tomography. *Ann. Vasc. Surg.* 65, 174–182. doi:10.1016/j.avsg.2019.10.072